1	Ultrathin polyorganosilica membranes synthesized by oxygen-plasma treatment of
2	polysiloxanes for H ₂ /CO ₂ separation
3	
4	Vinh Bui, ¹ Varun R. Satti, ¹ Elizabeth Haddad, ¹ Leiqing Hu, ¹ Erda Deng, ¹ Lingxiang Zhu, ² Won-
5	Il Lee, ³ Yifan Yin, ³ Kim Kisslinger, ⁴ Yugang Zhang, ⁴ Thomas T. Bui, ⁵ B. Medini Rajapakse, ⁵
6	Luis Velarde, ⁵ Chang-Yong Nam, ^{3,4} and Haiqing Lin* ¹
7	
8	¹ Department of Chemical and Biological Engineering, University at Buffalo, The State University
9	of New York, Buffalo, NY 14260, USA
10	² U.S. Department of Energy, National Energy Technology Laboratory, Pittsburgh, PA 15236,
11	USA
12	³ Department of Materials Science and Chemical Engineering, Stony Brook University, Stony
13	Brook, NY, 11794, USA
14	⁴ Center for Functional Nanomaterials, Brookhaven National Laboratory, Upton, NY, 11973, USA
15	⁵ Department of Chemistry, University at Buffalo, The State University of New York, Buffalo,
16	NY 14260, USA
17	
18	* Corresponding author: Haiqing Lin, E-mail: haiqingl@buffalo.edu
19	

Abstract

Oxygen plasma treatment of polydimethylsiloxane (PDMS) induces an ultrathin polyorganosilica (POSi) layer (< 10 nm) on top of a PDMS membrane, leading to excellent H₂/gas separation properties and providing a rapid and scalable way to fabricate robust silica membranes compared with conventional high-temperature and time-consuming sol-gel methods. Here, we thoroughly investigate POSi membranes derived from poly(dimethylsiloxane-*co*-methylhydroxidesiloxane) (poly(DMS-*co*-MHOS)) containing -SiOH groups that can be more easily converted to silica networks than the -SiCH₃ in PDMS. The effect of the polysiloxane structure and plasma treatment conditions (including plasma generating powers, oxygen flowrate, chamber pressure, and treatment time) on the silica chemistry, structure, and H₂/CO₂ separation properties are systematically determined to derive structure/property relationships. An optimized membrane exhibits H₂ permeance of 880 GPU and H₂/CO₂ selectivity of 67 at 150 °C, superior to state-of-the-art polymeric membranes. The membrane retains H₂/CO₂ selectivity as high as 46 when challenged with simulated syngas containing 2.8 mol% water vapor at 150 °C, demonstrating the potential of these POSi membranes for practical applications.

- Keywords: Polyorganosilica membranes; Oxygen plasma treatment; H₂/CO₂ separation;
- 37 Polysiloxane; Silica.

1. Introduction

Silica-based membranes can achieve strong molecular sieving ability with exceptional H_2 /gas separation performance due to their unique pores that are permeable to H_2 but reject larger molecules [1-6]. For example, Si600 membrane was prepared by a sol-gel process at 600 °C and exhibited H_2 permeance of 1493 GPU (1 GPU = 10^{-6} cm³(STP) cm⁻² s⁻¹ cmHg⁻¹) and H_2 /CO₂ selectivity of 71 at 200 °C [5], making it very attractive for industrial H_2 purification and precombustion carbon capture [7-11]. However, their production scale-up remains challenging due to the multi-cycles of high-temperature treatment and the easy formation of defects during the solgel process.

Rapid, low-temperature plasma technology has been developed to synthesize silica membranes and achieve superior separation properties [12-16]. Particularly, we reported a facile and scalable fabrication of polyorganosilica membranes (POSi) via room-temperature oxygen plasma treatment of polydimethylsiloxane (PDMS)-based thin-film composite (TFC) membranes using an inductively coupled plasma (ICP) - reactive ion etching (RIE) [2]. The ICP-RIE generated oxygen radicals and ions, which cleaved methyl groups on the PDMS backbones, forming Si-O-Si linkages and thus an ultrathin silica layer (<10 nm) within 360 s. The membrane exhibited an excellent H₂/CO₂ selectivity of 61 and moderate H₂ permeance of 100 - 300 GPU at 150 °C. However, the plasma treatment conditions, such as ICP and RIE input powers, chamber pressure, plasma exposure time, and oxygen flowrate, have not been optimized, and their effects on the membrane structures and separation properties have not been elucidated. Additionally, the structures and separation properties of the POSi membranes also depend sensitively on the polymer precursors [1, 17].

Here, we design and synthesize POSi membranes using poly(dimethylsiloxane-co-methylhydroxidesiloxane) or poly(DMS-co-MHOS) (Fig. 1a). The polysiloxane precursor contains -Si-OH groups to be more readily converted to -Si-O- groups than the -SiCH₃ in PDMS. This forms a POSi layer with a unique and uniform porous structure for precise H₂/CO₂ separation (Fig. 1a). The effect of plasma processing parameters on the membrane structures and separation properties is systematically investigated. The membrane surface chemistry was characterized using X-ray photoelectron spectroscopy (XPS), vibrational sum frequency generation (vSFG) spectroscopy, and a contact angle goniometer, and the surface structure was characterized using Atomic Force Microscope (AFM) and Grazing-Incidence Wide-Angle X-ray Scattering (GIWAXS). Pure- and mixed-gas H₂/CO₂ separation performance at various pressures was evaluated to derive the structure/property relationship and demonstrate their potential for industrial applications.

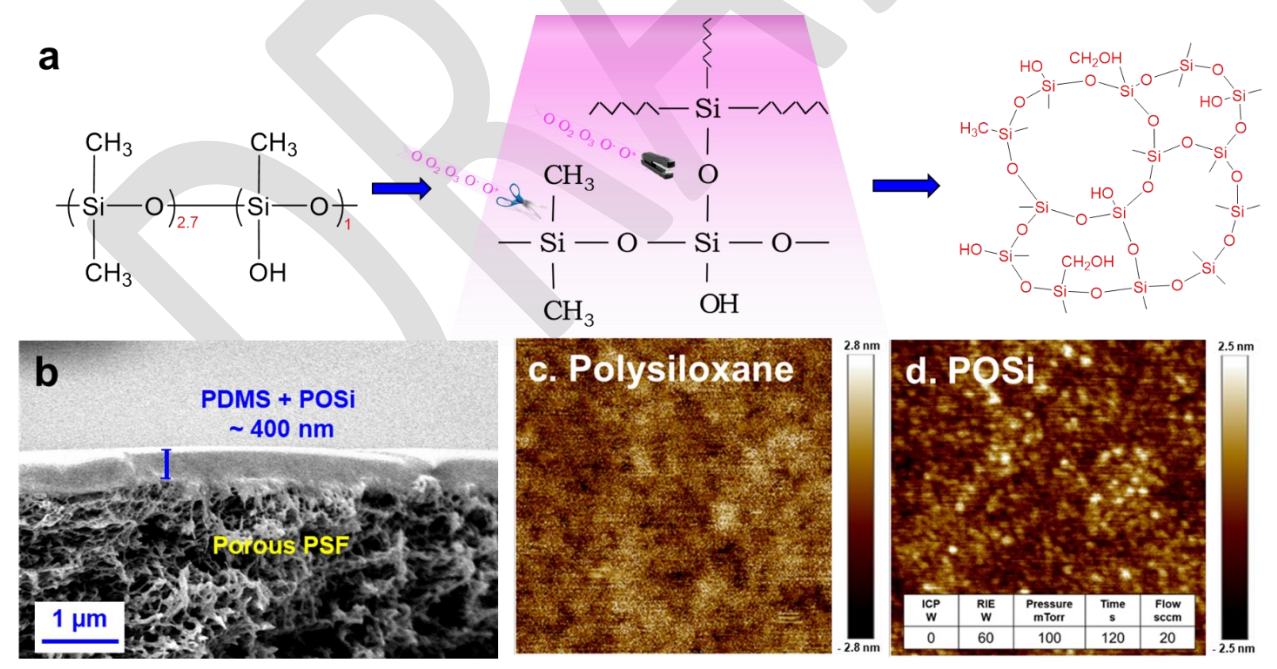


Fig. 1. Synthesis of ultrathin POSi membranes from poly(DMS-co-MHOS). (a) Conversion of polysiloxane to POSi via oxygen plasma exposure. (b) Cross-sectional SEM image of a POSi membrane. AFM surface images of (c) poly(DMS-co-MHOS) and (d) POSi membrane.

2. Experimental

2.1. Materials

Polysulfone (PSF) porous support with a molecular weight cut-off of 20 kDa was provided by Solecta, Inc. (Oceanside, CA). Wacker Dehesive 944 (30 mass% of vinyl-functionalized PDMS or vPDMS in toluene), Cross-linker V 24 (polymethylhydrosiloxane or PMHS), and Catalyst OL (1 mass% Platinum in vPDMS) were supplied by Wacker Chemical Corporation (Ann Arbor, MI). Isopropanol (IPA) and isooctane were provided by Fisher Scientific (Hampton, NH). Hexane was purchased from VWR International (Radnor, PA). Ultrahigh purity (> 99.999%) gas cylinders of H₂, CO₂, and N₂ were acquired from Airgas USA (Buffalo, NY).

2.2. Preparation of POSi membranes

POSi membranes were fabricated in three steps, including pre-treatment of PSF support, dip-coating of the polysiloxane precursor, and oxygen plasma treatment [2]. First, the PSF support was immersed in water for 1 day to remove the pore preservers, IPA for another day, and then isooctane for one more day before drying [18]. Second, ≈0.83 mass% poly(DMS-*co*-MHS) solution in hexane/toluene was prepared by mixing PDMS, PMHS, and OL at a mass ratio of 63: 23:14. The vinyl groups of PDMS react with the -SiH groups of PMHS by hydrosilylation [19]. Due to the excess amount of PMHS, the unreacted Si-H groups can react with water or O₂ to convert to Si-OH during the synthesis [20], producing poly(DMS-*co*-MHOS), which is confirmed by the disappearance of the Si-H groups on the Fourier Transform Infrared (FTIR) spectra (Fig. S1). The resulting copolymer has a mass ratio of PDMS to PMHOS of 72: 28 (or 10: 3) or a molar ratio of 2.7: 1. Third, the polysiloxane solution was coated onto the PSF support using a dip coater (MTI Corporation, Richmond, CA) with a soaking time of 5 s and a drawing speed of 5 cm/min. Finally, the membranes were treated by oxygen plasma in Phantom III (Trion Technology, Inc.,

Clearwater, FL) with controlled parameters, including RIE power, ICP power, exposure time, O₂ flowrate, and chamber pressure.

2.3 Membrane characterization

Water contact angle (WCA) was measured using a goniometer (Model 190, Rame Hart Instrument Co., Succasunna, NJ) with 2 µL water drops. Eight measurements were taken, and an average is reported. The vSFG measurements were conducted using a home-built femtosecond spectrometer with the detailed set-up and data collection shown in the Supplementary Information [21, 22]. The samples were coated on quartz plates to eliminate substrate interference.

AFM was conducted using Bruker Dimension Icon with ScanAsyst[®]. GIWAXS patterns were collected at the 11-BM Complex Materials Scattering (CMS) beamline of National Synchrotron Light Source II (NSLS-II) (with a wavelength of 0.9184 Å) at Brookhaven National Laboratory (Upton, NY). XPS was performed using a PHI5000 VersaProbe III scanning probe (Physical Electronics Inc., Chanhassen, MN) with a spot size of 100 μm, and at least three spots were analyzed for each sample. Atomic concentrations and peak deconvolutions were calculated using the CasaXPS package. For the AFM, XPS, and GIWAXS analysis, polysiloxane and POSi samples were prepared on Si wafers.

The membrane cross-section was imaged using a focused ion beam scanning electron microscope (FIB-SEM) (Carl Zeiss Auriga CrossBeam, Germany). X-ray diffraction (XRD) patterns were collected using Rigaku Ultima IV X-ray diffractometer (Rigaku Analytical Devices, MA) with the Cu Kα X-ray wavenumber of 1.54 Å⁻¹.

Pure-gas permeance was determined at 5.1 atm and 150 °C using a constant-volume and variable-pressure apparatus [2, 23]. Mixed-gas separation properties were determined by a constant-pressure and variable-volume apparatus at 4.4 atm and 150 °C with a feed flowrate of

200 cm³(STP) min⁻¹ (sccm) to achieve a stage-cut of less than 1% [24]. Water vapor was introduced into the feed by passing through a bubbler at 23, 50, and 70 °C to attain water vapor content of 0.63 mol%, 2.8 mol% and 7.0 mol%, respectively. Nitrogen was used as a sweep gas on the permeate side with the flowrate of 2 - 10 sccm. The permeate composition was analyzed using a Micro GC 3000 gas analyzer (Inficon Inc., East Syracuse, NY). The uncertainty of gas permeance and H₂/CO₂ selectivity are estimated to 10% and 14%, respectively, using the error propagation method [25].

3. Results and discussion

3.1. Membrane characterization

Fig. 1b presents the cross-sectional SEM image of a POSi membrane, where the combined thickness of the POSi and poly(DMS-co-MHOS) layer is \approx 400 nm. The POSi layer is expected to be very thin (10 nm or less) and indistinguishable from the polysiloxane layer [2]. The AFM images show that both polysiloxane and POSi have a smooth surface with a roughness value (Ra) of 1.4 and 0.6 nm, respectively (Fig. 1c).

The XPS analysis shows that polysiloxane exhibits an O/Si ratio of 1.29 ± 0.07 (sample #0 in Table S1), close to the theoretical value of 1.27 for poly(DMS-co-MHOS) (Fig. 1a). On the other hand, the C/Si ratio of 2.06 ± 0.04 is greater than the theoretical value of 1.73, partially because of the vinyl groups in the vPDMS used.

Fig. 2a compares the Si 2p and C1s peaks of the poly(DMS-co-MHOS) and POSi samples. The Si 2p peaks are deconvoluted into three peaks at 102.1, 102.8, and 103.4 eV, corresponding to Si(-O)₂, Si(-O)₃, and Si(-O)₄, respectively, while the C 1s peaks are deconvoluted into C-H at 284.6 eV and C-O at 286 eV [2, 26]. The pristine polysiloxane exhibits the characteristic peaks of

Si(-O)₂ and Si(-O)₃ with the Si(-O)₂ being the prominent component in the Si 2p region and only C-H contribution in C 1s region. By contrast, the POSi shows existence of Si(-O)₄ and C-O, confirming the methyl scission and oxidation in generating the silica structures [2, 26-28].

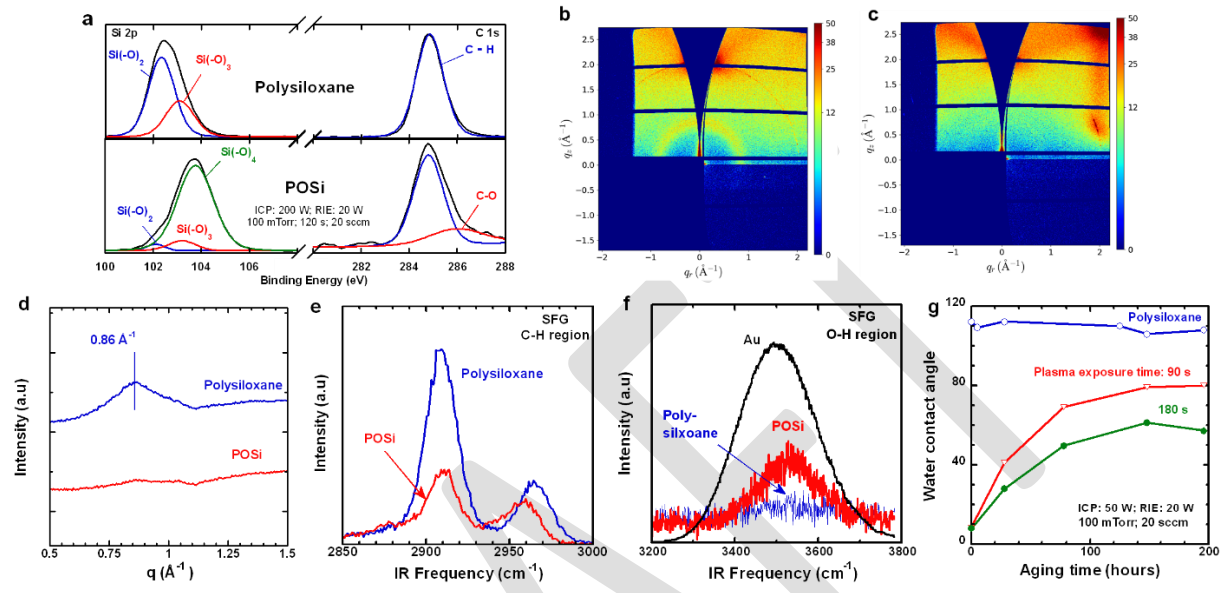


Fig. 2. Surface comparison of poly(DMS-co-MHOS) and POSi #20. (a) Deconvolution of Si 2p and C 1s for the XPS patterns. 2D GIWAXS patterns of (b) polysiloxane and (c) POSi at a penetration depth of 8.1 nm. (d) Reduced 1D GIWAXS curves obtained by circular average of 2D GIWAXS pattern at a penetration depth of 8.1 nm. The vSFG patterns in (e) the C-H and (f) O-H region, where the non-resonant SFG response of gold (Au, bandwidth ~400 cm⁻¹) represents the IR energy profile used in the experiment. (g) WCA as a function of the aging time.

Fig. 2b displays GIWAXS pattern of the polysiloxane at an incident angle of 0.08° (corresponding to a penetration depth of 8.1 nm). The sample exhibits a peak at $q_x = 0.86 \text{ Å}^{-1}$ (as determined by 1D GIWAXS curves, Fig. 2d), which corresponds to a d-spacing of 7.3 Å calculated using Bragg's equation. This peak can be attributed to the ribbon like conformation of the folded PDMS chains, which assemble into a lamella-like structure [29]. This characteristic peak of PDMS is also observed on the XRD pattern at 2 θ of 11.7° (d-spacing of 7.6 Å, Fig. S2) [30]. After exposure to oxygen plasma, the polysiloxane peak is suppressed (Fig. 2c), suggesting the

conversion of the polysiloxane to the amorphous silica structure. Fig. 2d also suggests that the POSi layer is thicker than the penetration depth (\approx 8.1 nm).

Fig. 2e,f presents the surface vSFG patterns in the C-H and O-H region of the polysiloxane and POSi, respectively. The polysiloxane shows stronger peaks of methyl symmetric stretching (CH₃-SS) at 2909 cm⁻¹ and methyl anti-symmetric stretching (CH₃-AS) at 2965 cm⁻¹ [31] than the POSi because of the decreased methyl groups after the oxygen plasma treatment. Furthermore, the POSi exhibits an increase in H-bonded vicinal silanol characteristic peak centered at ~3540 cm⁻¹ (Fig. 2f), suggesting the insertion of oxygen atoms into the POSi layer [32]. These results further validate the methyl scission and oxidation of polysiloxane to produce silica.

Fig. 2g compares the WCA of the polysiloxane and POSi as a function of the aging time at ≈ 23 °C. The oxygen plasma treatment of 90 and 180 s reduces the WCA from $110^{\circ} \pm 2^{\circ}$ to $< 10^{\circ}$ initially (Fig. S3), indicating an increased hydrophilicity [2, 16]. However, the WCA of the POSi samples increases with time because of the silanol condensation [14, 28] or diffusion of low molecular weight PDMS from the bulk to the surface over time [33]. Similar behaviors were observed for other POSi samples (Fig. S4b-f), though the polysiloxane shows constant WCAs with time. Nevertheless, the hydrophobic recovery in the POSi does not affect their gas transport properties as evidenced by the stable gas permeation properties right after the plasma treatment, indicating the dominant role of the silica phase (Section 3.4).

3.2. Effect of plasma treatment time and oxygen pressure and flowrate on POSi membranes

Fig. 3a,b presents the effect of the plasma exposure time on H₂/CO₂ separation properties at 5.1 atm and 150 °C. Increasing the plasma exposure time decreases H₂ permeance and increases H₂/CO₂ selectivity at different chamber pressures. For instance, increasing the exposure time from 120 to 360 s at 100 mTorr (or 13.3 Pa) decreases H₂ permeance from 1160 to 570 GPU and

increases H₂/CO₂ selectivity from 23 to 42, which can be attributed to the increased degree of polysiloxane to POSi conversion, as evidenced by the increased O/Si from 2.14 to 2.69 and decreased C/Si ratio from 0.80 to 0.32 (samples #9 and #11 in Table S1, respectively). Furthermore, the Si(-O)₄ peak contribution increases from 70.5% to 76.4%, and the C-H peak contribution decreases from 85.7% to 70.1% (Fig. 3c and Tables S2 and S3), consistent with the enhanced formation of silica structures.

Fig. S5 presents the gas permanence and H₂/gas selectivity of POSi membrane as a function of the penetrant kinetic diameter. Increasing the penetrant kinetic diameter from 2.89 Å (H₂) to 3.8 Å (CH₄) dramatically decreases gas permeance from 730 to 3.7 GPU. Additionally, the membrane shows H₂/CH₄ selectivity of 196, much higher than H₂/CO₂ (28), suggesting the gas separation is dominated by molecular sieving mechanism [2].

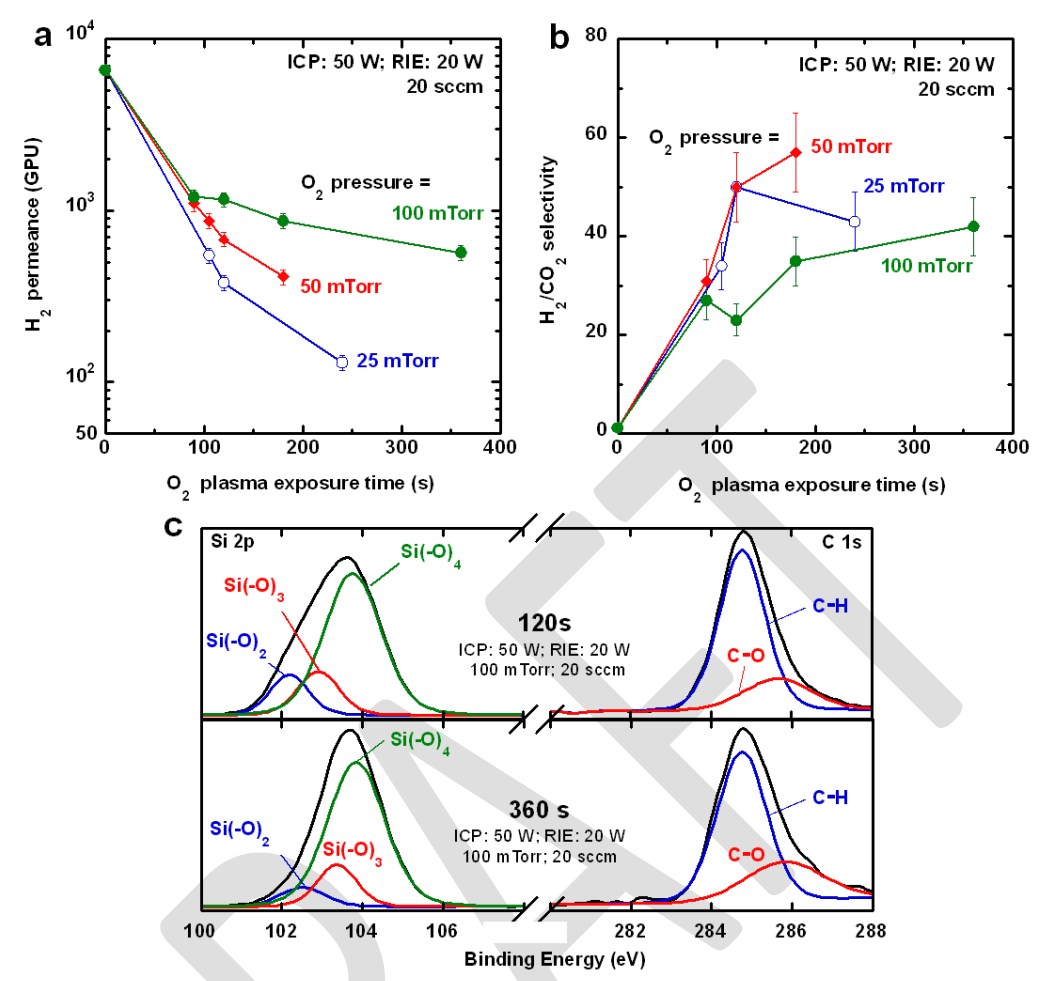


Fig. 3. Influence of oxygen plasma exposure time on (a) pure-gas H_2 permeance and (b) H_2/CO_2 selectivity at 5.1 atm and 150 °C. (c) Surface chemistry determined by XPS of the POSi membranes prepared at plasma exposure time of 120 and 360 s. The membranes were prepared with ICP of 50 W, RIE of 20 W, and O_2 flowrate of 20 sccm at 100 mTorr.

Fig. 4a illustrates the effect of the oxygen flowrate on H₂/CO₂ separation properties. The polysiloxane membrane is denoted with 0 sccm oxygen flowrate. Increasing the oxygen flowrate decreases H₂ permeance and increases H₂/CO₂ selectivity before leveling off at an oxygen flowrate of 10 sccm. For instance, increasing oxygen flowrate from 0 to 10 sccm rapidly enhances the H₂/CO₂ selectivity from 1.2 to 48 and reduces H₂ permeance from 6600 to 640 GPU because of the formation of the silica layer. By contrast, increasing the oxygen flowrate from 20 to 98 sccm exerts a negligible impact on POSi chemical structure and H₂/CO₂ transport properties. For

example, XPS surface analysis shows similar O/Si ratio values of 2.18 and 2.1 for POSi prepared at 20 and 98 sccm, respectively (sample #6 and #15 in Table S1, respectively) and similar Si(-O)₄ peak contribution of ≈83% (Fig. 4b and Table S2).

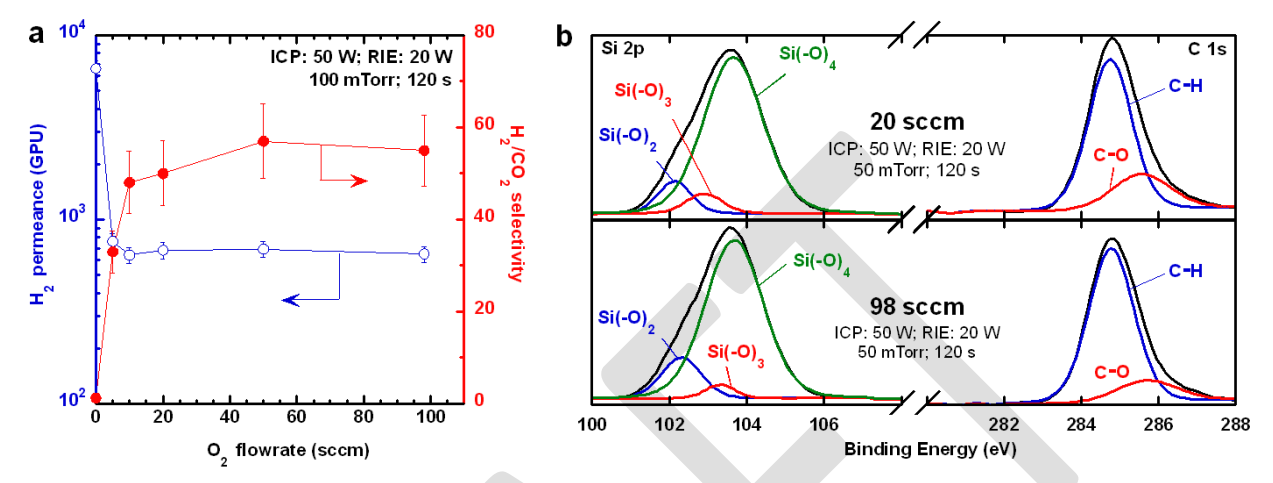


Fig. 4. Effect of the oxygen flowrate on (a) pure-gas H₂/CO₂ separation properties at 5.1 atm and 150 °C and (b) surface chemistry determined by XPS. The membranes were prepared with ICP of 50 W, RIE of 20 W, chamber pressure of 50 mTorr and plasma exposure time of 120 s.

Fig. 5a displays the effect of the chamber pressure on H₂/CO₂ separation properties. Increasing the chamber pressure from 50 mTorr (sample #6 in Table S1) to 500 mTorr (sample #16) increases H₂ permeance from 680 to 1700 GPU and decreases H₂/CO₂ selectivity from 50 to 15. However, both samples exhibit almost the same O/Si and C/Si ratios (Table S1) and Si(-O)₄ peak contribution (Fig. 5b and Table S2), suggesting similar silica structures. On the other hand, higher chamber pressure often leads to lower oxygen ion energy with broader energy distribution due to the greater collision rate between ions and neutral species [34, 35], and therefore, increasing the chamber pressure could decrease the silica layer thickness [36], resulting in higher H₂ permeance and lower H₂/CO₂ selectivity. However, the silica layer in both membranes is too thin to determine for validation in this study.

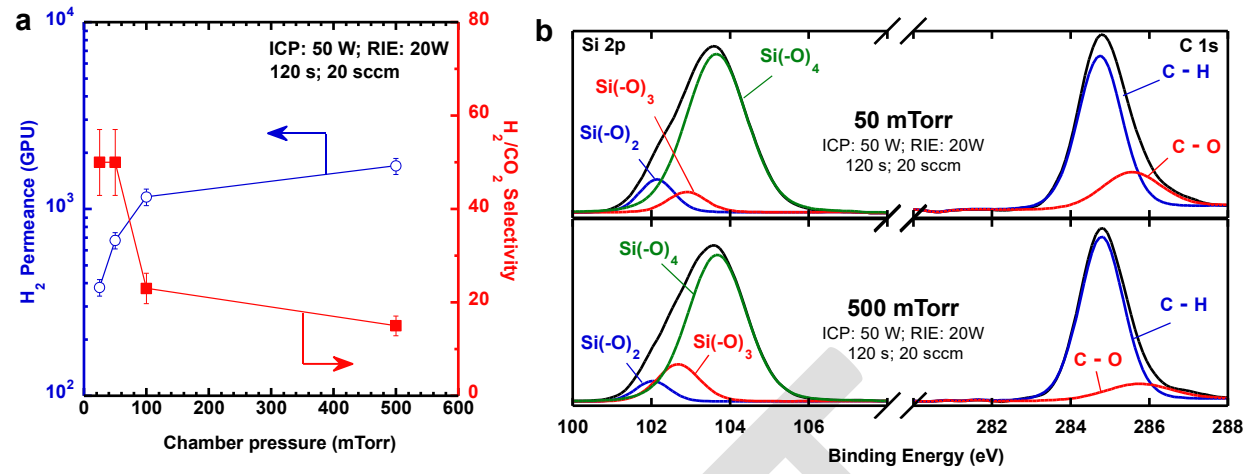


Fig. 5. Effect of the chamber pressure on (a) pure-gas H₂/CO₂ separation properties at 5.1 atm and 150 °C and (b) membrane surface chemistry determined by XPS. The membranes were prepared with ICP of 50 W, RIE of 20 W, plasma exposure time of 120 s, and O₂ flowrate of 20 sccm.

3.3. Effect of the ICP-RIE powers on POSi membranes

RIE and ICP are two independent plasma generation processes, where RIE mode generates low density plasma with high ion bombardment energy due to the directional electric field generated from the electrodes. An increase in RIE power increases the plasma density and ion bombardment energy. On the other hand, ICP mode generates higher plasma density with lower ion bombardment energy. The combined ICP-RIE allows independent control of plasma density (ICP input power) and ion bombardment energy (RIE input power) [37]. However, there is a delicate balance in our process, i.e., the use of plasma to generate silica layer [2] and the etching of the silica layer by the same plasma [38]. As such, the effect of the ICP-RIE powers on the membrane structure and performance can be complex.

To investigate the influence of different plasma generation modes on membrane separation performance, plasma treatment was conducted with one plasma mode at one time. Fig. 6a presents the effect of the ICP power on H₂/CO₂ separation properties and membrane structure at RIE power of 0 W. Increasing the ICP power from 50 W (sample #36 in Table S1) to 200 W (sample #39) decreases H₂ permeance from 2000 to 990 GPU and increases H₂/CO₂ selectivity from 11 to 36,

consistent with the increased O/Si content from 2.35 to 2.46, decreased C/Si ratio from 0.88 to 0.66, and increased Si(-O)₄ peak contribution from 58.6% to 72.3% (Fig. 6c and Table S2) because of the higher oxygen ionization at higher ICP power [34, 39, 40], leading to thicker silica layers with fewer micro-defects.

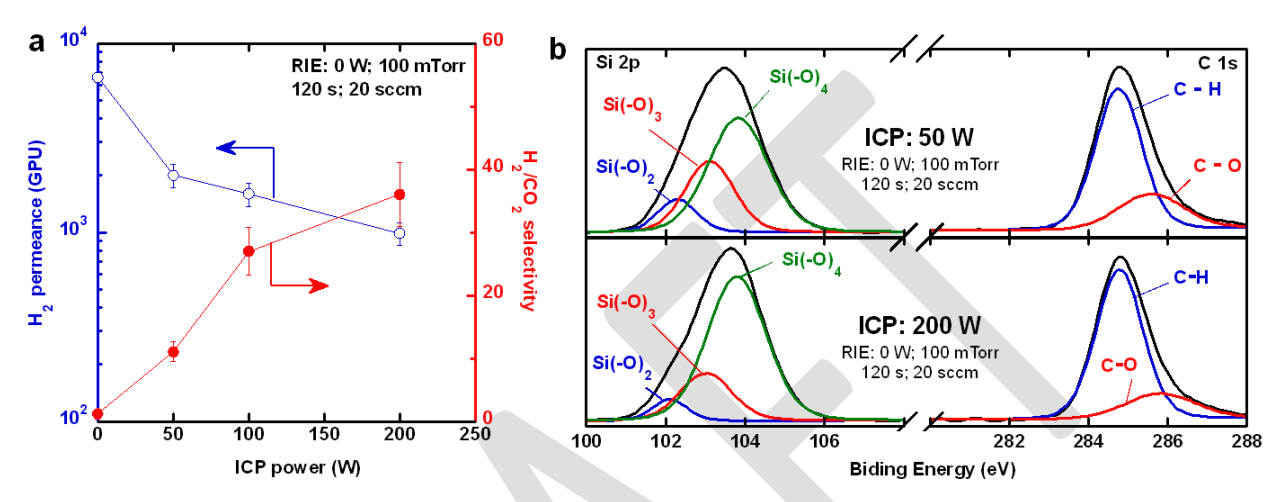


Fig. 6. Influence of the ICP power on (a) H_2/CO_2 separation properties at 5.1 atm and 150 °C and (b) membrane surface chemistry determined by XPS. The membranes were prepared with RIE of 20 W at 100 mTorr, plasma exposure time of 120 s, and O_2 flowrate of 20 sccm.

Fig. 7 displays the effect of the RIE power on the H₂/CO₂ separation properties and surface chemistry with the ICP power of 0 W. Increasing the RIE power from 10 to 60 W drastically decreases H₂ permeance from 1800 to 77 GPU, while the H₂/CO₂ selectivity exhibits a peak of 53 at an RIE power of 20 W (Table S5). The decreased H₂ permeance and the initial increase in H₂/CO₂ selectivity can be ascribed to the increased silica formation, as evidenced by the increase of the Si(-O)₄ content from 0 (polysiloxane, sample #0 in Table S2) to 18.8 mol% (POSi with 20 W of RIE, sample #27). The decrease in H₂/CO₂ selectivity at RIE of 40 and 60 W is probably caused by micro-defects induced from greater ion bombardment at higher RIE power [41-43]. However, these micro-defects cannot be visualized.

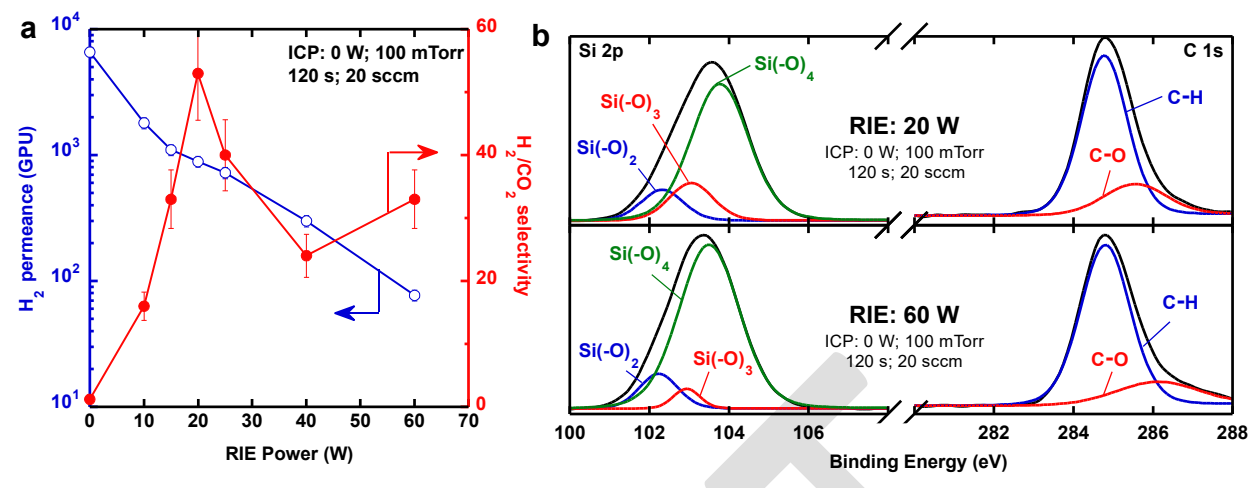


Fig. 7. Influence of the RIE power on (a) H₂/CO₂ separation properties at 5.1 atm and 150 °C and (b) surface chemistry determined by XPS. The membranes were prepared with ICP of 0 W, plasma treatment time of 120 s, and O₂ flowrate of 20 sccm at 100 mTorr.

Interestingly, when both plasma generation modes are employed, irregular trends are observed for H₂/CO₂ separation properties (Fig. 8 and Tables S5 and S6). With an RIE power of 20 W, increasing the ICP power from 0 to 50 W increases H₂ permeance from 890 to 1160 GPU and decreases H₂/CO₂ selectivity from 53 to 23, but a further increase of the ICP to 200 W decreases H₂ permeance to 890 GPU and increases H₂/CO₂ selectivity to 67. These behaviors can be explained as follows. First, at an ICP power of 0, the surface modification is dominated by the RIE plasma mode (20 W). Second, at the ICP power of 50 W or above, the plasma process is dominated by the ICP plasma mode (consistent with the increased Si(-O)₄ contribution from 71% at 50 W to 89% at 200 W, as shown in Fig. 8b and Table S2), leading to an increased H₂/CO₂ selectivity with increasing ICP power.

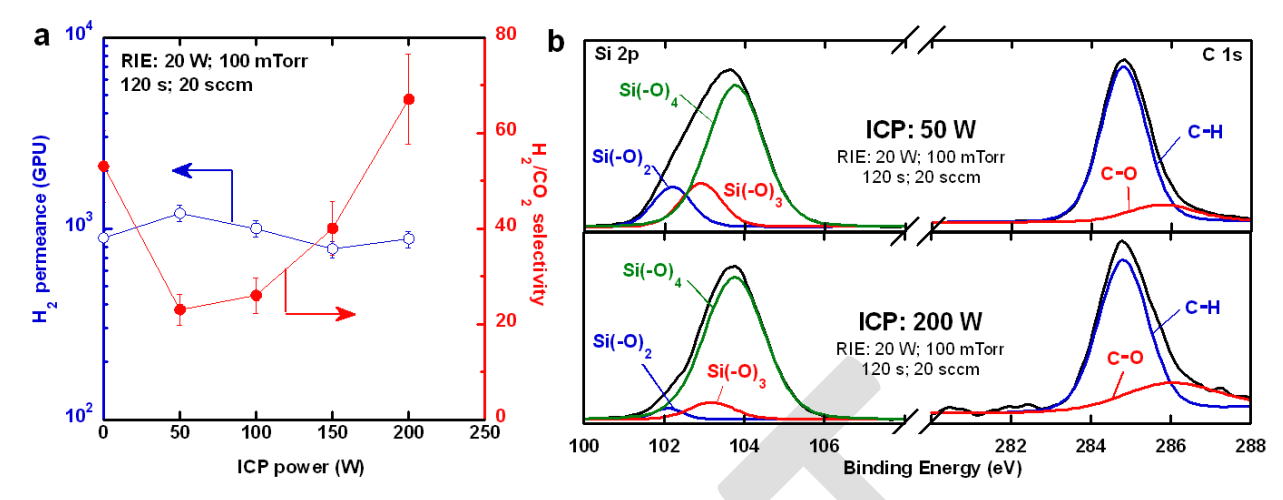


Fig. 8. Coupling effect of the ICP and RIE power on (a) H₂/CO₂ separation properties at 150 °C and (b) surface chemistry determined by XPS. The membranes were prepared with RIE of 20 W at 100 mTorr, plasma treatment time of 120 s, and O₂ flowrate of 20 sccm.

The coupling effect of the ICP and RIE on the plasma generation regime and thus the H₂/CO₂ separation properties can also be observed for a constant ICP of 50 W and RIE power ranging from 0 to 60 W (Fig. S6). Increasing the RIE power from 20 to 60 W gradually increases the H₂/CO₂ selectivity from 23 to 34 and decreases H₂ permeance from 1200 to 170 GPU because of the increased silica formation. The absence of the maximum selectivity (observed in Fig. 7a) at RIE of 20W is probably caused by the high ICP power (50 W), resulting in the separation performance trend like that observed in the single-mode study of the ICP.

The effect of the RIE power on the H_2/CO_2 separation properties can also be characterized using plasma dosing (PD_{RIE}), i.e., the number of ions and radicals that the membrane surface is exposed to. The PD_{RIE} can be estimated using Equation 1:

$$298 PD_{RIE} = \frac{RIE \times t}{p_{O_2}} (1)$$

where t is the exposure time (s), and p_{O_2} is the O_2 pressure (mTorr). This estimation is reasonable because the plasma ion density and kinetic energy are directly proportional to the power [34, 39,

40], and they decrease with increasing O_2 pressure [34, 35, 39]. The PD_{RIE} does not consider the O_2 flowrate as most membranes in this study were prepared at 20 sccm (Table S4).

Fig. 9 illustrates a reasonably good correlation between the PD_{RIE} and H_2/CO_2 separation properties at a constant ICP of 50 W, i.e., increasing the PD_{RIE} decreases H_2 permeance (with $R^2 = 0.81$) and increases H_2/CO_2 selectivity (with $R^2 = 0.43$), consistent with the improved formation of the silica structures. By contrast, Fig. S7 shows that there are no good correlations between H_2/CO_2 separation properties and the total plasma dosing (such as the sum of ICP and RIE power) or the ICP dosing (at an RIE of 20 W). These results can be ascribed to the complexity of the oxygen plasma ionization, where ions with different chemical activities (such as charges and spinning orientation) and densities depend sensitively on the processing parameters determining silica structures [39, 40]. By contrast, the RIE power plays a critical role in determining the ion bombardment energy [44, 45], which can directly promote ion penetration into the polysiloxane and induce thicker silica layers [36], leading to decreased permeance at higher PD_{RIE} values.

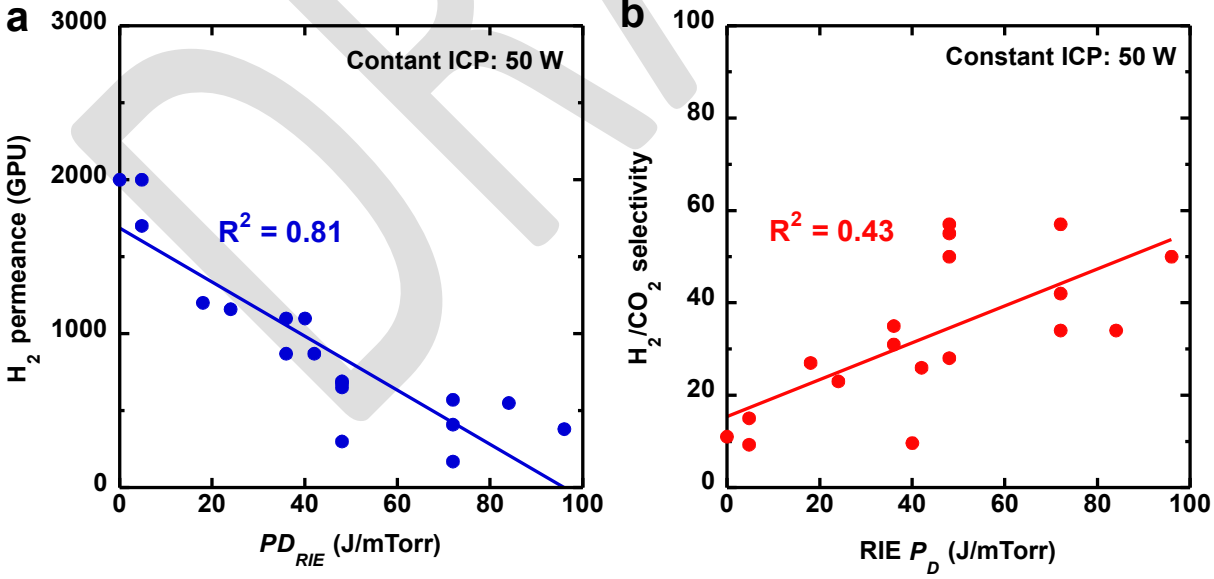


Fig. 9. Empirical correlation of the PD_{RIE} and (a) pure-gas H₂ permeance and (b) H₂/CO₂ selectivity at 5.1 atm and 150 °C for the POSi membranes at ICP = 50 W.

3.4. Superior H₂/CO₂ separation performance in POSi membranes

Fig. 10a demonstrates the flexibility in fine-tuning POSi structures and thus H₂/CO₂ separation properties at 150 °C by optimizing the oxygen plasma treatment conditions. The optimization starts with sample S (sample #20 in Table S4) because of its balanced H₂ permeance (880 GPU) and H₂/CO₂ selectivity (67). Then, the plasma treatment parameters are optimized based on the observed trends. For example, increasing the plasma exposure time from 120 to 360 s enhances H₂/CO₂ selectivity to 102 but reduces H₂ permeance to 340 GPU; decreasing the chamber pressure to 50 mTorr increases H₂/CO₂ selectivity to 77 but decreases H₂ permeance to 480 GPU; and increasing RIE power to 60 W increases H₂/CO₂ selectivity to 81 and decreases H₂ permeance to 88 GPU. Interestingly, increasing the ICP power to 400 W does not change H₂/CO₂ selectivity (67) but lowers H₂ permeance to 370 GPU. Nevertheless, all membranes show the H₂/CO₂ separation properties surpassing Robeson's upper bound, and this low-level optimization confirms the correlation between the plasma processing parameters and the separation properties.

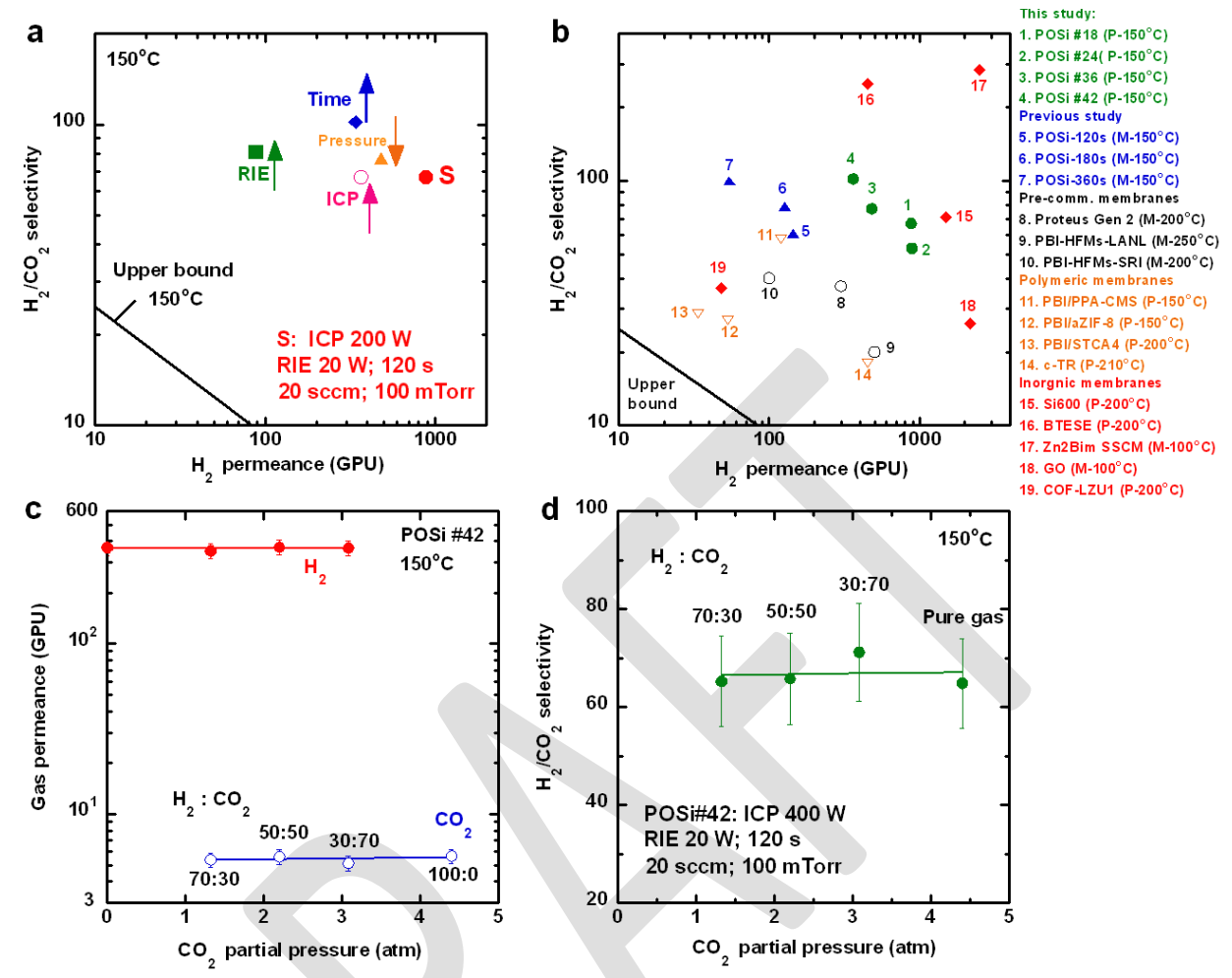


Fig. 10. Superior H₂/CO₂ separation properties in POSi membranes at 150 °C. (a) Flexibility in fine-turning separation properties by optimizing plasma treatment conditions based on sample S. (b) Comparison with state-of-the-art membranes reported in the literature and Robeson's upper bound estimated assuming 1-μm thick selective layers [9]. The "P" and "M" denote pure- and mixed-gas data, respectively. (c) Pure- and mixed-gas H₂ and CO₂ permeance and (d) H₂/CO₂ selectivity as a function of CO₂ partial pressure.

Fig. 10b compares the pure-gas H₂/CO₂ separation performance of POSi membranes against Robeson's upper bound and the leading membranes or materials. The upper bound was drawn assuming that the materials can be fabricated into TFC membranes with 1-μm thick selective layers. This assumption is reasonable, considering the challenge in the fabrication of defect-free thin films and physical aging for the glassy polymers or MMMs. The following observations are made. First, compared with the PDMS-derived POSi membranes [2], the

poly(DMS-co-PMOS)-derived POSi membranes exhibit much higher H₂ permeance and slightly lower H₂/CO₂ selectivity at similar plasma treatment conditions (Fig. S8) due to the competing effects of the loose polymer chain packing (caused by the short chains of PMHS [46]) and readily available Si-OH to form Si-O-Si networks and strong size-sieving ability. For instance, the sample S in this study exhibits H₂ permeance more than six times of the PDMS-derived POSi (880 GPU versus 144 GPU) and similar H₂/CO₂ selectivity (67 versus 61).

Second, our POSi membranes exhibit H₂/CO₂ separation performance superior to commercial membranes such as Proteus Gen 2 [47], pre-commercial membranes such as PBI hollow fiber membranes [9], and the state-of-the-art polymeric materials, such as PBI/PPA-based carbon molecular sieves (CMS) [10] and PBI/STCA4 [48]. POSi membranes also exhibit better separation properties than organosilica membranes derived from BTESE [49] but slightly lower performance than TEOS-derived membranes (Si600) [5]. On the other hand, inorganic membranes, such as Zn₂BIM₄ soft-solid MOF composite membranes [50], GO membranes [51], and TpTG_{Cl}@TpPa-SO₃H/COF-LZU1 [52], showed exceptional H₂/CO₂ separation properties, though they are difficult to be fabricated into industrial membranes on a large scale.

To investigate the POSi membrane's applicability to syngas separation, POSi #46 (Table S4) with a balanced H_2/CO_2 separation properties was further evaluated with different H_2/CO_2 gas mixtures in the presence of water vapor. Fig. 10c,d presents the gas permeance and H_2/CO_2 selectivity at 150 °C as a function of CO_2 partial pressure. The POSi membrane demonstrates separation performance independent of CO_2 partial pressure with H_2 permeance remaining at \approx 360 GPU and H_2/CO_2 selectivity at \approx 68, indicating its resistance to plasticization or competitive sorption.

Fig. 11 displays the long-term stability of POSi #46 in a continuous test with dry and wet gas at 150 °C. First, the membrane was subjected to the mixed-gas study with various gas mixtures for ≈ 48 h (Fig. 10c,d). The feed gas was then switched to H₂/CO₂ mixture of 50:50 at 4.4 atm for 24 h. During this 3-day test, the POSi exhibited stable H₂ permeance of ≈370 GPU and H₂/CO₂ selectivity of \approx 68, indicating its good resistance against aging. Second, water vapor at various contents (0.68, 2.8 and 7.0 mol%) was introduced to the H₂:CO₂ mixture to systematically evaluate their effect on H₂/CO₂ separation properties. At water vapor of 0.63 mol%, H₂ permeance initially decreased to 330 GPU, and H₂/CO₂ selectivity decreased to 52, but then they remained stable for 48 h. When the feed was shifted back to the dry condition, the membrane recovered H₂ permeance to 340 GPU and H₂/CO₂ selectivity to 55. Then the water vapor content was increased to 2.8 mol%, and H₂ permeance decreased to 255 GPU, and H₂/CO₂ selectivity decreased to 45 at 232nd hour. However, shifting back to the dry condition only recovered H₂ permeance to 310 GPU and H₂/CO₂ selectivity to 52. Finally, the POSi membrane was exposed to 7.0 mol% water vapor, which drastically decreased H₂ permeance to 180 GPU and H₂/CO₂ selectivity to 28. The POSi performance did not recover upon shifting back to the dry condition. Similar phenomena have been observed for POSi #20, which shows a decreased H₂ permeance from 690 to 460 GPU and H₂/CO₂ selectivity from 50 to 43 when exposed to 0.63 mol% of water vapor (Fig. S9) because of the simultaneous hydrolysis and condensation and thus the densification of the structures [1, 53-56]. By contrast, the pristine polysiloxane membrane exhibits almost the same H₂/CO₂ separation properties when exposed to 0.63 mol% water vapor (Fig. S10), confirming the detrimental effect on the silica structure (instead of the polysiloxane) by water vapor. Our future studies will focus on the improvement of the hydrothermal stability of the POSi membranes, following strategies

367

368

369

370

371

372

373

374

375

376

377

378

379

380

381

382

383

384

385

386

387

successfully adopted for silica membranes synthesized using the conventional sol-gel processes [1].

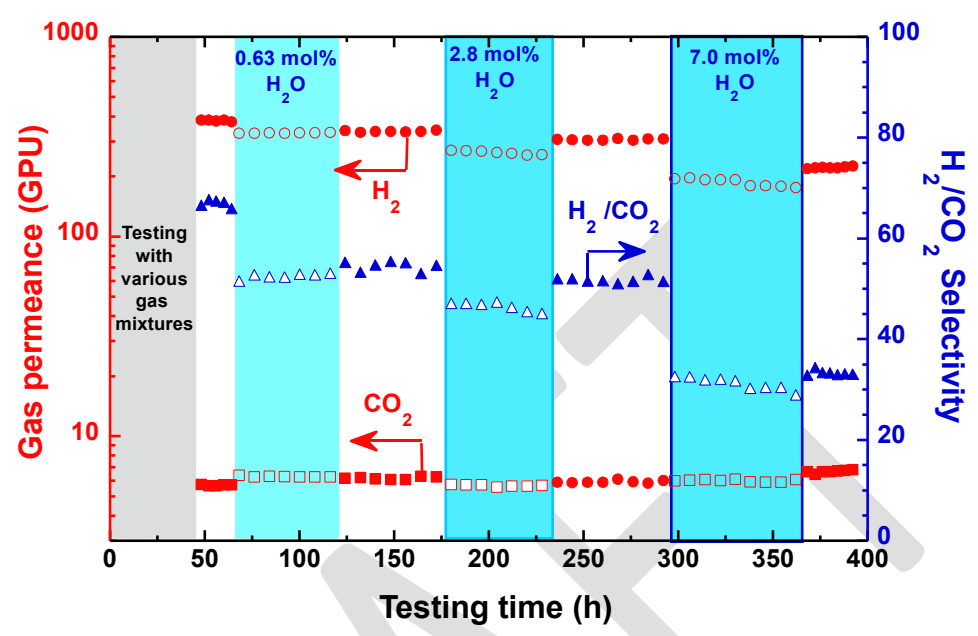


Fig. 11. Long term stability tests of the POSi #46 with dry and wet binary gas mixtures containing 50% H₂ and 50% CO₂ at 4.4 atm and 150 °C.

4. Conclusion

We demonstrate rapid fabrication of ultrathin POSi composite membranes by oxygen plasma treatment of poly(DMS-co-MHOS) with remarkable H₂/CO₂ separation performance. The successful synthesis of POSi layers is confirmed by XPS, vSFG, and GIWAXS, and the effect of a variety of synthesis parameters on the silica structure and H₂/CO₂ separation properties is summarized below.

- 1. POSi membranes derived from poly(DMS-co-MHOS) exhibit H₂ permeance 2 to 5 times higher and H₂/CO₂ selectivity slightly lower than those derived from PDMS prepared with similar plasma treatment conditions.
- 2. Increasing plasma exposure time decreases gas permeance and increases H₂/CO₂ selectivity because of the increased silica formation.

- 3. Increasing oxygen pressure increases gas permeance and decreases H₂/CO₂ selectivity because of the decreased silica formation.
- 4. Increasing oxygen flowrate decreases gas permeance and increases H₂/CO₂ selectivity beforing
 leveling off at 10 sccm.
- 5. Increasing the ICP power decreases gas permeance and increases H₂/CO₂ selectivity because of the increased silica formation.
- 412 6. Increasing the RIE power decreases H₂ permeance but increases H₂/CO₂ selectivity before 413 decreasing. There appears to be a reasonably good correlation between H₂/CO₂ separation 414 properties and the RIE-based plasma dosing.
- 7. A coupling effect between ICP and RIE plasma modes results in peculiar gas permeance and selectivity trends because of the competing effects of silica formation and etching by the same plasma dosing.

The POSi membranes exhibit H₂ permeance ranging from 300 to 900 GPU and H₂/CO₂ selectivity reaching 100 at 150 °C, superior to state-of-the-art commercial membranes and polymeric materials and far surpassing Robeson's upper bound. The membranes show stable separation performance when tested with dry gas mixtures. However, the presence of water vapor in the feed decreases both H₂ permeance and H₂/CO₂ selectivity, suggesting that silica structures with better resistance to hydrolysis will be needed for practical applications, or the feed gas streams need to be dehydrated before being introduced to the POSi membrane systems.

Acknowledgments

418

419

420

421

422

423

424

425

426

427

428

We gratefully acknowledge the financial support from the U.S. National Science Foundation (2044623 and 1753207). This research used the Materials Synthesis and

- 429 Characterization and Electron Microscopy Facilities of the Center for Functional Nanomaterials,
- 430 which is a U.S. DOE Office of Science Facility, at Brookhaven National Laboratory under
- 431 Contract No. DE-SC0012704.

433

434

Appendix A. Supplementary data

Supplementary data to this article can be found online at

435

436

References

- V. Bui, A. M. Tandel, V. R. Satti, E. Haddad, H. Lin. Engineering silica membranes for separation performance, hydrothermal stability, and production scalability. Adv. Membr. 3 (2023) 100064, 10.1016/j.advmem.2023.100064.
- 440 [2] L. Zhu, L. Huang, S. R. Venna, A. K. Blevins, Y. Ding, D. P. Hopkinson, M. T. Swihart, 441 H. Lin. Scalable polymeric few-nanometer organosilica membranes with hydrothermal 442 stability for selective hydrogen separation. ACS Nano. 15 (2021) 12119–12128, 443 10.1021/acsnano.1c03492.
- S. O. Lawal, L. Yu, H. Nagasawa, T. Tsuru, M. Kanezashi. A carbon–silica–zirconia ceramic membrane with CO₂ flow-switching behaviour promising versatile high-temperature H₂/CO₂ separation. J. Mater. Chem. A. 8 (2020) 23563-23573, 10.1039/D0TA07065C.
- 448 [4] M. Kanezashi, K. Yada, T. Yoshioka, T. Tsuru. Design of silica networks for development 449 of highly permeable hydrogen separation membranes with hydrothermal stability. J. Am. 450 Chem. Soc. 131 (2009) 414-415, 10.1021/ja806762q.
- 451 [5] R. M. De Vos, H. Verweij. High-selectivity, high-flux silica membranes for gas separation. 452 Science. 279 (1998) 1710-1711, 10.1126/science.279.5357.1710.
- 453 [6] P. Karakiliç, C. Huiskes, M. W. J. Luiten-Olieman, A. Nijmeijer, L. Winnubst. Sol-gel 454 processed magnesium-doped silica membranes with improved H₂/CO₂ separation. J. 455 Membr. Sci. 543 (2017) 195-201, 10.1016/j.memsci.2017.08.055.
- 456 [7] Y. Han, W. W. Ho. Polymeric membranes for CO₂ separation and capture. J. Membr. Sci. 628 (2021) 119244, 10.1016/j.memsci.2021.119244.
- T. C. Merkel, M. Zhou, R. W. Baker. Carbon dioxide capture with membranes at an IGCC power plant. J. Membr. Sci. 389 (2012) 441-450, 10.1016/j.memsci.2011.11.012.
- 460 [9] L. Hu, S. Pal, H. Nguyen, V. Bui, H. Lin. Molecularly engineering polymeric membranes for H₂/CO₂ separation at 100–300 °C. J. Polym. Sci. 58 (2020) 2467-2481, 10.1002/pol.20200220.
- L. Hu, V. T. Bui, A. Krishnamurthy, S. Fan, W. Guo, S. Pal, X. Chen, G. Zhang, Y. Ding, R. P. Singh. Tailoring sub-3.3 Å ultramicropores in advanced carbon molecular sieve membranes for blue hydrogen production. Sci. Adv. 8 (2022) eabl8160, 10.1126/sciadv.abl8160.

- G. Chen, T. Wang, G. Zhang, G. Liu, W. Jin. Membrane materials targeting carbon capture and utilization. Adv. Membr. 2 (2022) 100025, 10.1016/j.advmem.2022.100025.
- H. Nagasawa, R. Yasunari, M. Kawasaki, M. Kanezashi, T. Tsuru. Facile low-temperature route toward the development of polymer-supported silica-based membranes for gas separation via atmospheric-pressure plasma-enhanced chemical vapor deposition. J. Membr. Sci. 638 (2021) 119709, 10.1016/j.memsci.2021.119709.
- J. Rubner, S. Skribbe, H. Roth, L. Kleines, R. Dahlmann, M. Wessling. On the Mixed Gas Behavior of Organosilica Membranes Fabricated by Plasma-Enhanced Chemical Vapor Deposition (PECVD). Membranes. 12 (2022) 994, 10.3390/membranes12100994.
- 476 [14] S. Aoyama, H. Nagasawa, M. Kanezashi, T. Tsuru. Nanogradient hydrophilic/hydrophobic organosilica membranes developed by atmospheric-pressure plasma to enhance pervaporation performance. ACS Nano. 16 (2022) 10302-10313, 10.1021/acsnano.1c11656.
- 480 [15] J.-T. Chen, Y.-J. Fu, K.-L. Tung, S.-H. Huang, W.-S. Hung, S. Jessie Lue, C.-C. Hu, K.-481 R. Lee, J.-Y. Lai. Surface modification of poly(dimethylsiloxane) by atmospheric pressure 482 high temperature plasma torch to prepare high-performance gas separation membranes. J. 483 Membr. Sci. 440 (2013) 1-8, 10.1016/j.memsci.2013.03.058.
- 484 [16] J. Liu, Y. Pan, J. Xu, Z. Wang, H. Zhu, G. Liu, J. Zhong, W. Jin. Introducing amphipathic copolymer into intermediate layer to fabricate ultra-thin Pebax composite membrane for efficient CO₂ capture. J. Membr. Sci. 667 (2023) 121183, 10.1016/j.memsci.2022.121183.
- 487 [17] X. Ren, T. Tsuru. Organosilica-based membranes in gas and liquid-phase separation.
 488 Membranes. 9 (2019) 107, 10.3390/membranes9090107.
- 489 [18] G. Zhang, V. T. Bui, Y. Yin, E. H. R. Tsai, C.-Y. Nam, H. Lin. Carbon Capture Membranes 490 Based on Amorphous Polyether Nanofilms Enabled by Thickness Confinement and 491 Interfacial Engineering. ACS Appl. Mater. Interfaces. 15 (2023) 35543-35551, 492 10.1021/acsami.3c07046.
- 493 [19] X. Li, M. Cao, H. Shan, F. Handan Tezel, B. Li. Facile and scalable fabrication of superhydrophobic and superoleophilic PDMS-*co*-PMHS coating on porous substrates for highly effective oil/water separation. Chem. Eng. J. 358 (2019) 1101-1113, 10.1016/j.cej.2018.10.097.
- 497 [20] A. Esteves, J. Brokken-Zijp, J. Laven, H. Huinink, N. Reuvers, M. Van, G. De With.
 498 Influence of cross-linker concentration on the cross-linking of PDMS and the network
 499 structures formed. Polymer. 50 (2009) 3955-3966, 10.1016/j.polymer.2009.06.022.
- 500 [21] S. Sengupta, L. Bromley Iii, L. Velarde. Aggregated States of Chalcogenorhodamine Dyes 501 on Nanocrystalline Titania Revealed by Doubly Resonant Sum Frequency Spectroscopy. 502 J. Phys. Chem. C. 121 (2017) 3424-3436, 10.1021/acs.jpcc.6b12166.
- 503 [22] T. T. Bui, L. A. Colón, L. Velarde. Intermolecular Interactions at the Silica-Liquid 504 Interface Modulate the Fermi Resonance Coupling in Surface Methanol. J. Phys. Chem. 505 (2021) 5695-5702, 10.1021/acs.jpclett.1c01015.
- K. M. Rodriguez, W. Wu, T. Alebrahim, Y. Cao, B. D. Freeman, D. Harrigan, M. Jhalaria, 506 [23] A. Kratochvil, S. Kumar, W. Lee, Y. Lee, H. Lin, J. M. Richardson, Q. Song, B. Sundell, 507 508 R. Thur, I. Vankelecom, A. Wang, C. Wiscount, J. Xingming, Z. P. Smith. Multi-Lab Study on the Pure-Gas Permeation of Commercial Polysulfone (PSF) Membranes: Measurement 509 Practices. Membr. 510 Standards and Best J. Sci. 659 (2022)120746. 511 10.1016/j.memsci.2022.120746.

- 512 [24] L. Hu, K. Chen, W. I. Lee, K. Kisslinger, C. Rumsey, S. Fan, V. T. Bui, N. Esmaeili, T. Tran, Y. Ding, M. Trebbin, C.-Y. Nam, M. T. Swihart, H. Lin. Palladium-Percolated Networks Enabled by Low Loadings of Branched Nanorods For Enhanced H₂ Separations. Adv. Mater. 35 (2023) 2301007, 10.1002/adma.202301007.
- 516 [25] P. R. Bevington, D. K. Robinson. Data Reduction and Error Analysis for the Physical Sciences. 2nd ed. New York: McGraw-Hill, Inc.; 1992.
- H. Hillborg, J. Ankner, U. W. Gedde, G. Smith, H. Yasuda, K. Wikström. Crosslinked polydimethylsiloxane exposed to oxygen plasma studied by neutron reflectometry and other surface specific techniques. Polymer. 41 (2000) 6851-6863, 10.1016/S0032-3861(00)00039-2.
- [27] M. J. Owen, P. J. Smith. Plasma treatment of polydimethylsiloxane. J. Adhes. Sci. Technol.
 8 (1994) 1063-1075, 10.1163/156856194X00942.
- 524 [28] M. Morra, E. Occhiello, R. Marola, F. Garbassi, P. Humphrey, D. Johnson. On the aging 525 of oxygen plasma-treated polydimethylsiloxane surfaces. J. Colloid Interface Sci. 137 526 (1990) 11-24, 10.1016/0021-9797(90)90038-P.
- 527 [29] F. Schilling, M. Gomez, A. Tonelli. Solid-state NMR observations of the crystalline conformation of poly(dimethylsiloxane). Macromolecules. 24 (1991) 6552-6553, 10.1021/ma00024a032.
- 530 [30] G. L. Jadav, V. K. Aswal, H. Bhatt, J. C. Chaudhari, P. S. Singh. Influence of film thickness 531 on the structure and properties of PDMS membrane. J. Membr. Sci. 415 (2012) 624-634, 532 10.1016/j.memsci.2012.05.043.
- 533 [31] H. Ye, Z. Gu, D. H. Gracias. Kinetics of ultraviolet and plasma surface modification of poly(dimethylsiloxane) probed by sum frequency vibrational spectroscopy. Langmuir. 22 (2006) 1863-1868, 10.1021/la052030r.
- L. Dalstein, E. Potapova, E. Tyrode. The elusive silica/water interface: Isolated silanols under water as revealed by vibrational sum frequency spectroscopy. Phys. Chem. Chem. Phys. 19 (2017) 10343-10349, 10.1039/C7CP01507K.
- 539 [33] J. Kim, M. K. Chaudhury, M. J. Owen, T. Orbeck. The mechanisms of hydrophobic recovery of polydimethylsiloxane elastomers exposed to partial electrical discharges. J. Colloid Interface Sci. 244 (2001) 200-207, 10.1006/jcis.2001.7909.
- J. T. Gudmundsson, A. Marakhtanov, K. Patel, V. Gopinath, M. Lieberman. On the plasma parameters of a planar inductive oxygen discharge. J. Phys. D. 33 (2000) 1323, 10.1088/0022-3727/33/11/311.
- 545 [35] S. Kechkar, P. Swift, S. Kelly, S. Kumar, S. Daniels, M. Turner. Investigation of the electron kinetics in O₂ capacitively coupled plasma with the use of a Langmuir probe. Plasma Sources Sci. Technol. 26 (2017) 065009, 10.1088/1361-6595/aa6c90.
- 548 [36] S. Béfahy, P. Lipnik, T. Pardoen, C. Nascimento, B. Patris, P. Bertrand, S. Yunus.
 549 Thickness and elastic modulus of plasma treated PDMS silica-like surface layer. Langmuir.
 550 26 (2010) 3372-3375, 10.1021/la903154y.
- 551 [37] V. M. Donnelly, A. Kornblit. Plasma etching: Yesterday, today, and tomorrow. J. Vac. Sci. Technol. A. 31 (2013), 10.1116/1.4819316.
- 553 [38] G. Abromavičius, T. Juodagalvis, R. Buzelis, K. Juškevičius, R. Drazdys, S. Kičas. Oxygen 554 plasma etching of fused silica substrates for high power laser optics. Appl. Surf. Sci. 453 555 (2018) 477-481, 0.1016/j.apsusc.2018.05.105.
- 556 [39] M. W. Kiehlbauch, D. B. Graves. Inductively coupled plasmas in oxygen: Modeling and experiment. J. Vac. Sci. Technol. 21 (2003) 660-670, 10.1116/1.1564024.

- 558 [40] R. Zaplotnik, A. Vesel, M. Mozetic. Transition from E to H mode in inductively coupled oxygen plasma: Hysteresis and the behaviour of oxygen atom density. EPL. 95 (2011) 55001, 10.1209/0295-5075/95/55001.
- D. Bodas, J.-Y. Rauch, C. Khan-Malek. Surface modification and aging studies of additioncuring silicone rubbers by oxygen plasma. Eur. Polym. J. 44 (2008) 2130-2139, 10.1016/j.eurpolymj.2008.04.012.
- D. Bodas, C. Khan-Malek. Hydrophilization and hydrophobic recovery of PDMS by oxygen plasma and chemical treatment—An SEM investigation. Sens. Actuators B Chem. 123 (2007) 368-373, 10.1016/j.snb.2006.08.037.
- S. Bhattacharya, A. Datta, J. M. Berg, S. Gangopadhyay. Studies on surface wettability of 567 [43] 568 poly (dimethyl) siloxane (PDMS) and glass under oxygen-plasma treatment and correlation Microelectromech. 569 with bond strength. J. Syst. 14 (2005)590-597, 570 10.1109/JMEMS.2005.844746.
- 571 [44] K. Racka-Szmidt, B. Stonio, J. Żelazko, M. Filipiak, M. Sochacki. A review: Inductively coupled plasma reactive ion etching of silicon carbide. Materials. 15 (2021) 123, 10.3390/ma15010123.
- 574 [45] H.-C. Lee. Review of inductively coupled plasmas: Nano-applications and bistable hysteresis physics. Appl. Phys. Rev. 5 (2018) 011108, 10.1063/1.5012001.
- 576 [46] S. J. Lue, C. L. Tsai, D.-T. Lee, K. Mahesh, M. Y. Hua, C.-C. Hu, Y. Jean, K.-R. Lee, J.-577 Y. Lai. Sorption, diffusion, and perm-selectivity of toluene vapor/nitrogen mixtures 578 through polydimethylsiloxane membranes with two cross-linker densities. J. Membr. Sci. 579 349 (2010) 321-332, 10.1016/j.memsci.2009.11.064.
- J. Kniep, W. Salim, T. Merkel, C. Casillas, K. Amo, J. He, I. Huang, V. Nguyen, V. Batoon. Bench-scale development of a transformative membrane process for pre-combustion CO₂ capture. Membrane Technology and Research, Inc., Newark, CA (United States); 2022.
- J. Wu, C. Z. Liang, A. Naderi, T. S. Chung. Tunable supramolecular cavities molecularly homogenized in polymer membranes for ultraefficient precombustion CO₂ capture. Adv. Mater. 34 (2022) 2105156, 10.1002/adma.202105156.
- 586 [49] H. Song, Y. Wei, H. Qi. Tailoring pore structures to improve the permselectivity of organosilica membranes by tuning calcination parameters. J. Mater. Chem. A. 5 (2017) 24657-24666, 10.1039/c7ta07117e.
- 589 [50] L. Shu, Y. Peng, R. Yao, H. Song, C. Zhu, W. Yang. Flexible soft-solid metal—organic framework composite membranes for H₂/CO₂ separation. Angew. Chem. Int. Ed. 61 (2022) e202117577, 10.1002/anie.202117577.
- [51] H. Li, Z. Song, X. Zhang, Y. Huang, S. Li, Y. Mao, H. J. Ploehn, Y. Bao, M. Yu. Ultrathin,
 molecular-sieving graphene oxide membranes for selective hydrogen separation. Science.
 342 (2013) 95-98, 10.1126/science.1236686.
- 595 [52] Y. Ying, S. B. Peh, H. Yang, Z. Yang, D. Zhao. Ultrathin Covalent Organic Framework 596 Membranes via a Multi-Interfacial Engineering Strategy for Gas Separation. Adv. Mater. 597 34 (2022) 2104946, 10.1002/adma.202104946.
- 598 [53] M. Kanezashi, T. Matsutani, H. Nagasawa, T. Tsuru. Fluorine-induced microporous silica 599 membranes: Dramatic improvement in hydrothermal stability and pore size controllability 600 for highly permeable propylene/propane separation. J. Membr. Sci. 549 (2018) 111-119, 601 10.1016/j.memsci.2017.11.072.
- 602 [54] G. Gong, H. Nagasawa, M. Kanezashi, T. Tsuru. Tailoring the separation behavior of polymer-supported organosilica layered-hybrid membranes via facile Post-treatment using

- 604 HCl and HNO₃ vapors. ACS Appl. Mater. Interfaces. 8 (2016) 11060-11069, 10.1021/acsami.6b01986.
- 606 [55] M. Kanezashi, T. Shioda, T. Gunji, T. Tsuru. Gas permeation properties of silica 607 membranes with uniform pore sizes derived from polyhedral oligomeric silsesquioxane. 608 AIChE J. 58 (2012) 1733-1743, 10.1002/aic.12716.
- 609 [56] N. W. Ockwig, T. M. Nenoff. Membranes for hydrogen separation. Chem. Rev. 107 (2007) 4078-4110, 10.1021/cr0501792.